

Conformation and Dynamics of Poly(*N*-isopropyl acrylamide) Trimers in Water: A Molecular Dynamics and Metadynamics Simulation Study

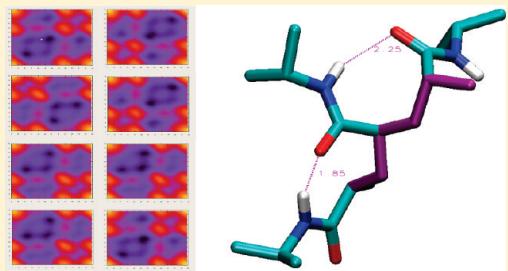
Emmanuel Autieri,[†] Ester Chiessi,^{*,†} Alice Lonardi,[†] Gaio Paradossi,[†] and Marcello Segà[‡]

[†]Department of Chemical Sciences and Technologies, University of Rome Tor Vergata, Via della Ricerca Scientifica I, 00133 Rome, Italy

[‡]Department of Physics, University of Trento, via Sommarive 14, 38123 Trento, Italy

 Supporting Information

ABSTRACT: Conformational features, structure, and dynamic properties of the trimer of poly(*N*-isopropyl acrylamide), (*NIPAAm*)₃, in aqueous solution at 293 and 323 K were investigated by a double simulation approach. The free energy behavior as a function of backbone conformation was obtained by metadynamics-umbrella sampling simulations. The structural characteristics, the intramolecular and water hydrogen bonding, and the torsional dynamics were analyzed by molecular dynamics simulations. The four stereoisomers of (*NIPAAm*)₃, representing syndiotactic, isotactic, and atactic sequences, were studied to highlight the tacticity effect on the system properties. The simulation results indicate that the experimentally observed lower hydrophilicity of isotactic poly(*N*-isopropyl acrylamide), in comparison with the syndiotactic one, is related to a lower conformational entropy. The atactic stereoisomers display the highest intramolecular hydrogen bond capability, at both studied temperatures, due to formation of hydrogen bonds between external amide groups. The mobility of the backbone in the syndiotactic trimer is more homogeneous than in other stereoisomers. The temperature increase was found mainly to affect the conformation of *N*-isopropyl amide side chains, and a structural rearrangement was observed for the atactic stereoisomers, in agreement with their experimental solution behavior. Simulation results are discussed in relation with available experimental data on solution properties and reactivity of poly(*N*-isopropyl acrylamide).



1. INTRODUCTION

The conformational preferences of macromolecules are dictated by steric requirements and by the possibility to establish nonbonding interactions (hydrogen bonds (HBs) and dipole–dipole) between repeating units. The interaction with the solvent can alter this scenario, especially for polymers with HB forming and/or hydrophobic groups in water. The case of poly(*N*-isopropyl acrylamide) (PNIPAAm) in aqueous solution is an example where each of these aspects plays a role.

PNIPAAm is one of the most popular synthetic macromolecules in the scientific literature of the last two decades. Since the first publications in 1956 about the synthesis and polymerization of the corresponding monomer, *N*-isopropyl acrylamide (NIPAAm),^{1–4} an increasing amount of papers has been reported on PNIPAAm.⁵ Particular attention has been devoted to its particular thermal behavior in aqueous media^{6,7} and, more recently, to the development of new hybrid PNIPAAm containing systems for different applications.^{8–11} Due to the amphiphilic character of PNIPAAm, with polar amide and nonpolar isopropyl groups, the polymer–water interaction is modulated by temperature and the hydrated state is thermodynamically favored below the so-called lower critical solution temperature (LCST), that lies between ca. 30 and 35 °C, the exact temperature depending on the degree of polymerization and the concentration of the polymer.^{12–14} Below the LCST, the aqueous solutions

of this macromolecule are stable and the networked systems based on PNIPAAm are swollen. Above the LCST, the solubility of PNIPAAm in water falls down, with a change of hydration state from a hydrophilic to a hydrophobic form in the surrounding of the LCST.¹⁵ The dehydration of PNIPAAm is concerted with a sharp conformational transition from relaxed coil to globule state,¹⁶ a process exploited to obtain reversible thermo-responsive polymer networks.^{17–19} Laser light scattering experiments on a single high molar mass PNIPAAm chain in aqueous solution indicate that the coil-to-globule and globule-to-coil transitions involve four distinct thermodynamically stable states of the macromolecule's global conformation.⁷

It is noteworthy that the macromolecular character of PNIPAAm is not a key factor for the LCST behavior of its aqueous solutions, since the same behavior is shown by aqueous solutions of short PNIPAAm oligomers^{13,14} and of *N*-isopropyl propionamide (NIPPA), the molecule corresponding to the repeating unit of PNIPAAm.^{12,20,21}

In spite of the huge amount of experimental studies on the phase transition phenomena of PNIPAAm solutions, the simulation investigations on this topic are relatively scarce. To our

Received: March 4, 2011

Revised: April 11, 2011

Published: April 25, 2011

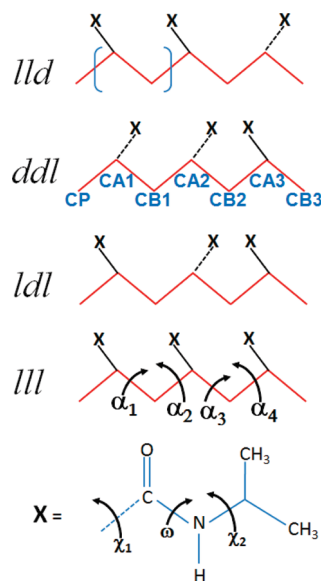
knowledge, three papers describing molecular dynamics (MD) simulations of PNIPAAm oligomers in water below and above the LCST^{22–24} and three MD studies on water and polymer properties in PNIPAAm networked systems^{25–28} appeared in the literature. MD simulation studies of the “monomer” NIPPA both in water²² and in water/methanol solutions²⁹ were recently published, the last paper being related to the reentrant coil-to-globule-to-coil transition behavior displayed by PNIPAAm in the mixed solvent.³⁰

The purpose of the present work is to highlight the leading factors for the conformational behavior of PNIPAAm in water. The conformational analysis of polymer systems was developed about 50 years ago, when it contributed to rationalize the conformational preferences of polypeptides, determining the secondary structure in proteins.³¹ The conformational theory was then applied to the structure of polysaccharides and extended to the study of the spatial configuration of polynucleotide chains, thus involving the other two classes of natural macromolecules.^{32,33} As far as vinyl polymers are concerned, the study of the conformational energy of linear³⁴ and branched³⁵ polyalkenes led to the rotational isomeric state (RIS) model for chain molecules.³⁶ The RIS model, together with statistical mechanical methods, was used to correlate the experimentally measured average dimension of the polymer chains in the unperturbed, random coil form with the chain structure and the steric hindrances associated with bond rotations.^{34,35} A reasonable agreement between experimental and calculated characteristic ratio and temperature coefficient of aliphatic linear vinyl polymers was reported by Flory et al.,³⁵ in a study where only the interactions between groups separated by three and by four C–C bonds (i.e., the interactions dependent on near-neighboring pairs of dihedral angles) were considered in the calculation of the weight of the rotational states.³⁵

The conformational behavior of PNIPAAm at room temperature was indirectly probed in previous experimental works regarding the rate of exchange of the N–H hydrogen in nonhelical polyamides,^{37,38} carried out to understand the exchange kinetics in proteins, where, differently from PNIPAAm, the amide group is in the main chain. Hydrogen–deuterium exchange was measured for PNIPAAm over a molecular weight (MW) range from 100 to 200 000 g/mol. A sharp drop in rate was found going from monomer to trimer, followed by a very slow progressive decrease at increasing MWs,³⁸ a behavior indicating that the local environment of the exchanging amide residue is largely established by the mutual interaction of as few as three residues. This result suggested to consider the trimer as the shortest oligomer with local structure and dynamics peculiar to the polymer. Therefore, taking into account these findings, we tackled the investigation of PNIPAAm conformational behavior by considering the PNIPAAm trimer, (NIPAAm)₃. To the aim of highlighting the effect of the chain stereochemistry on the conformational and solution properties, the study was carried out for all the stereoisomers of (NIPAAm)₃. In a very recent work,³⁹ PNIPAAm dimer model compounds were investigated with computational and experimental methods to understand the effect of tacticity on the polymer hydrophilicity. Here, we extend the analysis with a molecular approach to the PNIPAAm trimer, to relate structural properties of the oligomer with its water interaction.

In a double simulation scheme, we performed both metadynamics (MT) and classical molecular dynamics (MD) simulations, offering different but complementary information on PNIPAAm trimer in aqueous solution. MT simulations provided

Chart 1. Stereoisomers of (NIPAAm)₃



the conformational free energy as a function of the backbone dihedral angles, giving a static picture of the system in terms of the more stable conformers and the more favorable paths for conformational transitions. MD simulations added the information on dynamics and were used to explore the structural characteristics and the polymer–water interaction. To investigate the temperature effect, MT and MD simulations were carried out at 293 and 323 K, i.e., below and above the LCST of PNIPAAm in atactic configuration.

According to Flory's paper on the conformational statistics of vinyl polymers,³⁵ we found that the population of the isomeric rotational states is markedly affected by the stereochemical configuration of the –CHR– groups of the chain. Experimental studies on stereoregular PNIPAAm's, following the discovery of a new procedure for the stereocontrolled radical polymerization of acrylamides,⁴⁰ show that the phase boundary in water and the LCST are strongly influenced by the tacticity of PNIPAAm.^{41–44} The comparison between the results obtained at the two temperatures in the present study evidences a stereochemistry-dependent influence of temperature on the overall chain conformation and on the hydrophilicity of the trimers, in agreement with the experimental behavior of stereoregular PNIPAAm's in aqueous solution.

2. METHODS

2.1. Developing the Model. We considered the four stereoisomers of (NIPAAm)₃, shown schematically in Chart 1. The end-capping groups of the chain are a methyl group (named as CP in Chart 1) and a hydrogen atom. The sequence of the configuration of the residues (from left to right) is reported in Chart 1, naming as *l* (or *d*) a residue with the amide group exiting (or entering) the plane containing the backbone chain. Each trimer includes two adjacent dyads, meso or racemo, depending on whether the stereochemical configuration of near-neighbor –CHR– groups of the dyad is the same or opposite, respectively. For symmetry reasons, any other combination of configurations corresponds to a stereoisomer already included in Chart 1.

The initial structures of the trimers, in an *all-trans* conformation, were obtained using a program for molecular building of the

CHARMM software package,⁴⁵ starting from the internal coordinates of the residue. Each stereoisomer was energy minimized in vacuo using the conjugate gradient method with a maximum step size of 0.1 nm and a tolerance of 20 kJ·mol⁻¹·nm⁻¹; then, it was inserted into a cubic box of 2.5 nm side and solvated by about 500 SPC water molecules.⁴⁶ The energy of the hydrated systems was again minimized, before using them as starting configurations. The GROMOS force field G4SA3^{47,48} was used for this procedure and in the following MD and MT simulations, treating the aliphatic CH, CH₂, and CH₃ groups with the united-atom convention. The same force field was already successfully used in describing the hydrophobic collapse of longer PNIPAAm oligomers.²⁴ The box size was chosen to avoid interaction between periodic images. The preparation of the starting configurations was carried out by Compaq Alpha XP1000 and HP XW8600 workstations.

2.2. Simulation Procedures. *2.2.1. Molecular Dynamics Simulations.* MD simulations were carried out on the IBM BladeCenter LS21 Cluster at the CINECA Supercomputing Center (Bologna, Italy) with the GROMACS 3.3.3 program.^{49,50}

Simulations were performed in the NPT ensemble, using the leapfrog integration algorithm⁵¹ with a 2 fs time step. The cubic periodic boundary condition and minimum image convention were used, and the LINCS procedure⁵² was applied to constrain all bond lengths. The simulations were performed at 293 and 323 K by controlling the temperature with tBerendsen's coupling algorithm,⁵³ with a time constant of 0.1 ps. The pressure was maintained at 1.0 bar by a Berendsen isotropic coupling,⁵³ with a relaxation time of 0.5 ps. Electrostatic interactions were calculated by the smooth particle-mesh Ewald method,⁵⁴ the cutoff of nonbonded interactions being set to 1.2 nm. The total sampling for each stereoisomer was 40 ns at both temperatures.

In order to verify the reproducibility of the results, further independent 40 ns long trajectories were generated at 293 and 323 K for every stereoisomer, using the same starting configuration coordinates but different starting velocities. The atomic coordinates were saved every 2 ps for later analysis.

The graphic visualization was done using the molecular viewer software package VMD.⁵⁵

2.2.2. Metadynamics Simulations. In the past few years, a number of techniques have been proposed to enhance phase space sampling, especially in systems that show metastable states.^{56,57} MT, one of these methods,⁵⁸ introduces a biasing potential on a set of collective variables (CVs), $s(x)$, where x stands for the atomic coordinates, which represent all slow degrees of freedom of the system. The bias is realized by a history-dependent potential, $U_B(s(x), t)$, built up by adding Gaussian functions in the CV space. As a result of an MT run, the bias potential provides an estimate of the free energy surface $F(s)$ of the system with respect to the chosen collective variables, according to eq 1:

$$F(s) = -U_B(s) \quad (1)$$

This method can be refined combining the MT run with an umbrella sampling procedure. In such a scheme, described in detail in the papers of Babin et al.⁵⁹ and Segal et al.,⁶⁰ the MT run is followed by an umbrella sampling run that samples the probability density $\rho_B(s)$ of the biased system:

$$\rho_B(s) = \frac{e^{-\beta[F(s) + U_B(s)]}}{\int e^{-\beta[F(s) + U_B(s)]} ds} \quad (2)$$

with $\beta = (kT)^{-1}$. The final free energy profile is then obtained according to eq 3:

$$F(s) = -U_B(s) - kT \ln \rho_B(s) \quad (3)$$

where $U_B(s)$ is the free energy estimated by the metadynamics run and $\rho_B(s)$ derives from the following umbrella sampling procedure.

This combined simulation scheme removes possible systematic errors of the MT part and at the same time allows one to evaluate the statistic uncertainty on $F(s)$.

The collective variables chosen for our systems are the backbone torsional angles of (NIPAAm)₃, namely, the dihedral angles α_1 (CP—CA1—CB1—CA2), α_2 (CA1—CB1—CA2—CB2), α_3 (CB1—CA2—CB2—CA3), and α_4 (CA2—CB2—CA3—CB3), shown in Chart 1.

The MT-umbrella sampling runs were performed using the same parameters as reported in section 2.2.1, with the PLUMED⁶¹ (version 1.1.0) patch to the GROMACS software package (version 4.0.4).^{49,50,62,63}

The MT part of the run consisted of a 40 ns trajectory for each system, calculated by adding Gaussian terms of height 0.5 kJ/mol and width 0.1 rad for the angular variables every 250 integration steps. Separate two-dimensional free energy surfaces were calculated using as CVs the dihedral pairs at the junctions between the first and second residue and between the second and third residue, (α_1, α_2) and (α_3, α_4), respectively. Two different MT simulations of 20 ns were therefore calculated for each stereoisomer, using the same starting configuration, both at 293 and 323 K. It has to be emphasized that, in the most general case, if N slow degrees of freedom are present in the system, the definition of the M -dimensional free energy

$$F(s_1, \dots, s_M) = -kT \ln \int \exp[-\beta \cdot F(s_1, \dots, s_N)] ds_{M+1} \dots ds_N \quad (4)$$

with $M < N$, compulsorily requires the calculation of the complete N -dimensional free energy $F(s_1, \dots, s_N)$. In our case, however, the decomposition in dyads of $F(\alpha_1, \alpha_2, \alpha_3, \alpha_4)$ is a reasonable approximation, as metastabilities are not so severe. Indeed, MD runs of comparable length were found to sample about 90% of the dyads' profile populations obtained with MT (i.e., missing roughly 10% of possible conformers). This finding gives a rough idea of the inaccuracy which is introduced by performing the dyad decomposition in MT simulation: when one samples two CVs with MT, the other two CVs evolve according to unbiased MD, hence under-sampling the phase-space by the aforementioned 10%. This is the price in accuracy that we have to pay in order to perform a feasible two-dimensional MT, instead of a too computationally demanding four-dimensional MT. The specific choice of the pairs of consecutive dihedrals has been made to focus the single junction between adjacent residues, in order to highlight the influence of the stereochemistry of CHX neighboring groups and the tacticity effects within the dyad.

Finally, the umbrella sampling phase consisted of 40 ns MD runs, at the same thermodynamic conditions. During this phase, the histogram ρ_B was collected by sampling configurations every 0.1 ps on a grid of 100 points for all angles, in the range [0, 360]°.

The population probability of the thermodynamic states (free energy minima) was evaluated from the free energy profiles $F(\alpha_1, \alpha_2)$ and $F(\alpha_3, \alpha_4)$. For a given basin, S , of the $F(\alpha_1, \alpha_2)$

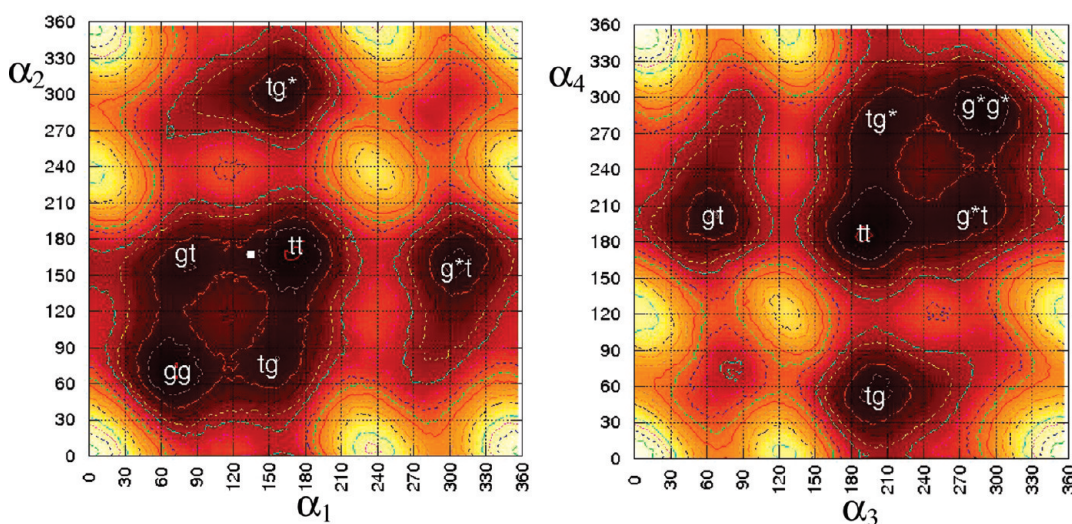


Figure 1. Free energy maps of the *ldl* stereoisomer at 293 K. Left side: $F(\alpha_1, \alpha_2)$; right side: $F(\alpha_3, \alpha_4)$. Energy contours are given at intervals of 10 kJ/mol relative to the *gg* state (left side) and *tt* state (right side).

profile, its probability can be calculated as

$$P(S) = \frac{\int_{D_S} e^{-\beta[F(\alpha_1, \alpha_2)]} d\alpha_1 d\alpha_2}{\int_{D_\Omega} e^{-\beta[F(\alpha_1, \alpha_2)]} d\alpha_1 d\alpha_2} \quad D_\Omega = [0, 360]^\circ \times [0, 360]^\circ$$

$$(5)$$

The domain D_S is a subset of the whole phase space D_Ω , representing the contour of the state basin S on the free energy profile. These contours were chosen as rectangles, with a direct cut along the axis direction. Determining with more care the contour, for example, by following isoergonic lines on the profile, did not give sensible correction, as the terms in the integral are exponentially suppressed with growing free energy. The corresponding analysis of the state probability was performed on the $F(\alpha_3, \alpha_4)$ profiles.

3. RESULTS AND DISCUSSION

3.1. Metadynamics Simulations. In the following discussion, we will adopt the RIS model nomenclature for the dihedral conformation, naming as *t* (trans), *g* (gauche), and *g** (gauche*) the conformations with a dihedral value around 180, 60, and 300°, respectively. Speaking of an *ij* conformational state of a dyad, the dihedral pair is meant as $\alpha_1\alpha_2$ or $\alpha_3\alpha_4$, depending on whether the dyad is formed by the first and second residue or by the second and third residue, respectively.

The conformational free energy profiles obtained for the *ldl* stereoisomer at 293 K are shown in Figure 1. In this stereoisomer, formed by two racemo dyads, the configuration sequence corresponds to the syndiotactic chain arrangement. It should be noted that the $F(\alpha_1, \alpha_2)$ and $F(\alpha_3, \alpha_4)$ maps of Figure 1 are related by a center of inversion in the origin, deriving from the symmetry relationship between the *ld* and *dl* enantiomeric pairs in *ldl*. The free energy profiles of the racemo dyads in this stereoisomer show two preferred conformational states, corresponding to the *tt* and *gg* dihedral pairs in *ld* (or *tt* and *g*g** in *dl*). These two states are almost degenerate in terms of free energy and cover approximately the 75% of the total conformers. In the

tt and *gg* (or *g*g**) conformations, the *N*-isopropyl amide groups of the racemo dyad come to stay apart from each other, by lowering the sterical hindrance of the substituents. The structures (a) and (b) in Figure 2 are two snapshots from the MD trajectory of *ldl* at 293 K, showing the trimer in the lowest free energy conformations. The MD results show that both the *tt* and *gg/g*g** states of *ldl* can be stabilized by intramolecular HBs but the *tt* conformation displays a higher HB ability, as reported in section 3.2. The other four minimum energy states of the maps in Figure 1 have free energy from 1.6 to 2.8 kT higher than that of the lowest energy state and population from about 4 to 10%.

Figure 3 shows the free energy profiles for the *lll* stereoisomer at 293 K. In this case, the stereochemistry of the residue sequence corresponds to the isotactic chain, with two following meso dyads. The two maps of Figure 3 are similar and show three preferred conformational states, corresponding to the pairs *gt*, *tg**, and *tt*. The *gt* and *tg** states have similar free energy, and they are practically equivalent for spatial arrangement of the *N*-isopropyl amide groups of the dyad. In these two minimum energy conformations, the *N*-isopropyl amide groups of the dyad face opposite sides of the average plane containing the backbone chain, as shown in structures (c) and (d) of Figure 2. The free energy of the *tt* state is about 0.4 kT higher than that of the lowest energy states, and in this minimum energy conformation, the dihedral angles of the dyad move from the 180° value to decrease the steric hindrance between substituents facing the same side of the vinyl chain. The populations of these three states account for about 97% of the total for the meso dyad. The other states in Figure 3 have about 4 kT higher free energy than the *tt* state and populations lower than 1%.

The stereoisomers *ddl* and *lld* are enantiomers, and their configuration sequence corresponds to an atactic trimer, with meso and racemo dyads described by the (α_1, α_2) and (α_3, α_4) dihedrals, respectively. The free energy maps of *lld* at 293 K are reported in Figure 4. The free energy profile of the meso dyad in *lld* displays a strong similarity with the profiles of *lll* shown in Figure 3, and the profile of the racemo dyad in *lld* is similar to that of $F(\alpha_1, \alpha_2)$ in Figure 1. These similarities indicate that the near-neighboring residue scarcely influences the

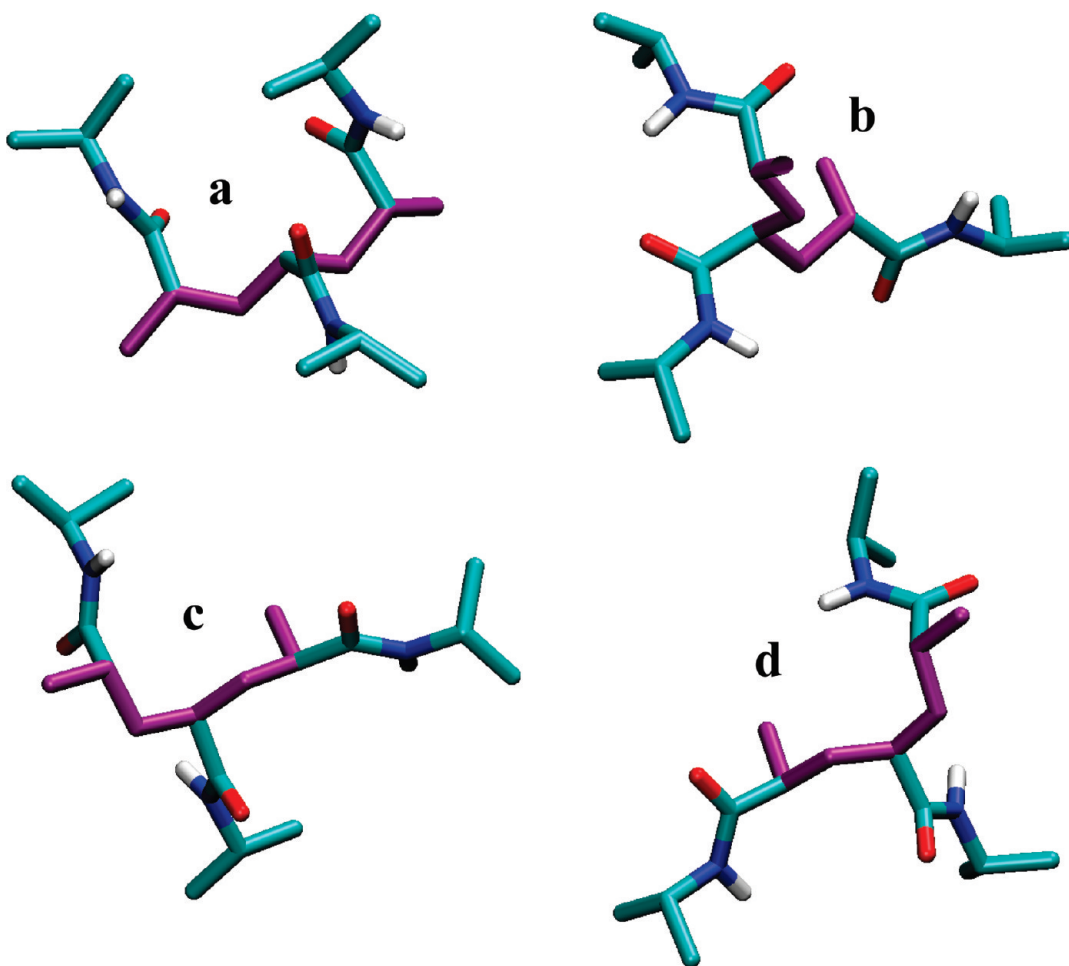


Figure 2. Stereoisomer *ldl* in *tt*–*tt* (a) and *tt*–*g***g** (b) conformations. Stereoisomer *llI* in *gt*–*gt* (c) and *tg**–*tg** (d) conformations. Snapshots from the MD trajectories at 293 K. The backbone chain is shown in purple. The conformation sequence is $\alpha_1\alpha_2-\alpha_3\alpha_4$.

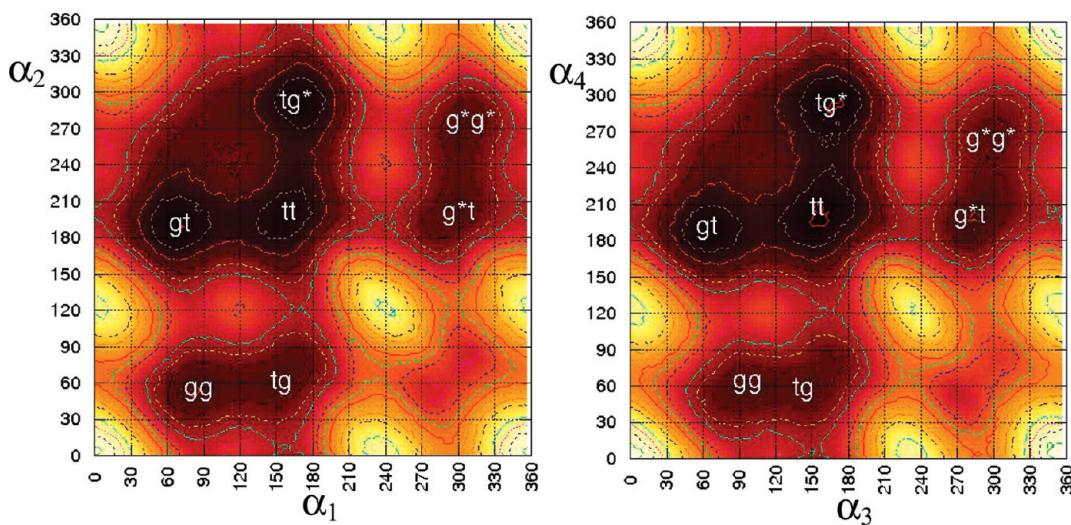


Figure 3. Free energy maps of the *llI* stereoisomer at 293 K. Left side: $F(\alpha_1, \alpha_2)$; right side: $F(\alpha_3, \alpha_4)$. Energy contours are given at intervals of 10 kJ/mol relative to the *gt* state (left side) and *tg** state (right side).

dyad's conformational behavior, mainly dictated by the sterical relationship between the adjacent *N*-isopropyl amide groups within the dyad considered. The free energy maps of

ddl at 293 K, shown in Part 1 of the Supporting Information, correspond to those of *lld*, taking into account the symmetry between the stereoisomers.

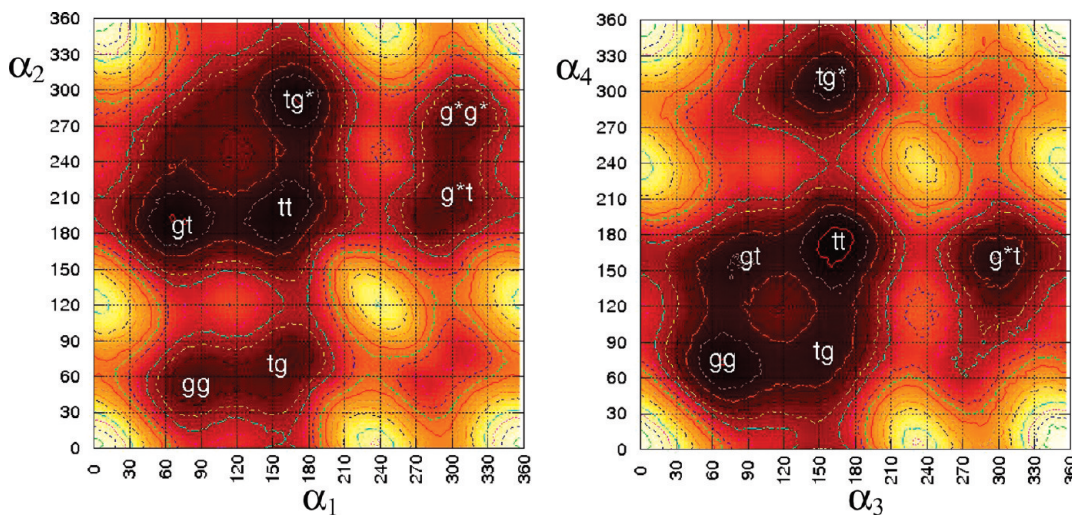


Figure 4. Free energy maps of the *lld* stereoisomer at 293 K. Left side: $F(\alpha_1, \alpha_2)$; right side: $F(\alpha_3, \alpha_4)$. Energy contours are given at intervals of 10 kJ/mol relative to the *gt* state (left side) and *tt* state (right side).

Table 1. Free Energy and Population Probability of the Conformational States for Meso Dyads, in Isotactic and Atactic Stereoisomers at 293 K

Isotactic Sequence							
<i>lll</i> – dyad 1–2 ^a			<i>lll</i> – dyad 2–3 ^b				
state ^c	coordinates ^d	F^e	state ^c	coordinates ^d	F^e		
gg	86;52	3.2(3)	0.84(1)	gg	97;63	4.8(3)	0.35(1)
tg	154;63	3.4(3)	0.65(1)	tg	143;57	5.1(3)	0.29(1)
gt	74;189	-0.7(3)	40.8(4)	gt	63;189	0.7(3)	20.4(4)
tt	160;200	0	31.2(4)	tt	154;206	0	42.9(5)
<i>g[*]t</i>	304;206	3.8(2)	0.55(1)	<i>g[*]t</i>	280;200	4.5(3)	0.64(1)
<i>tg[*]</i>	166;292	-0.3(3)	28.5(4)	<i>tg[*]</i>	166;292	-0.1(3)	35.3(6)
<i>g[*]g[*]</i>	310;275	4.0(2)	0.44(1)	<i>g[*]g[*]</i>	298;263	5.9(3)	0.15(1)

Atactic Sequence ^g							
<i>lld</i> – dyad 1–2 ^a			<i>ddl</i> – dyad 1–2 ^a				
state ^c	coordinates ^d	F^e	state ^c	coordinates ^d	F^e		
gg	86;52	4.4(2)	0.47(1)	<i>g[*]g[*]</i>	275;300	4.7(3)	0.33(1)
tg	154;69	4.1(2)	0.52(1)	<i>tg[*]</i>	200;290	4.1(3)	0.64(1)
gt	74;189	-0.4(3)	38.5(6)	<i>g[*]t</i>	290;160	-0.3(3)	34.8(7)
tt	160;200	0	31.3(4)	<i>tt</i>	206;166	0	30.6(5)
<i>g[*]t</i>	304;212	4.3(2)	0.50(1)	<i>gt</i>	63;160	3.6(3)	0.80(2)
<i>tg[*]</i>	172;292	-0.2(2)	28.4(4)	<i>tg</i>	190;63	-0.6(4)	32.2(7)
<i>g[*]g[*]</i>	310;280	4.5(3)	0.31(1)	<i>gg</i>	50;85	4.1(3)	0.36(1)

^aDyad formed by the first and second residues. ^bDyad formed by the second and third residues. ^cRIS nomenclature of the conformational state. ^dAngular coordinates (in degrees) of the absolute minimum of the basin. Pairs $\alpha_1;\alpha_2$ or $\alpha_3;\alpha_4$ for dyads 1–2 or 2–3, respectively. Errors within $\pm 6^\circ$. ^eFree energy (relative to the *tt* state), in kT units. ^fProbability in %. ^gThe states of *lld* and *ddl* corresponding for symmetry are reported in the same row.

In order to compare the conformational features of racemo and meso configurations in the different chain sequences, we report in Tables 1 and 2 the minimum free energy conformational states, their relative free energy and population, for the systems studied. The *tt* conformation was used as the free energy reference state, since it corresponds to the absolute minimum state for almost all racemo dyads and it is one of the lowest states for meso dyads. It is noteworthy that the *gg^{*}* and *g^{*}g^{*}*

Table 2. Free Energy and Population Probability of the Conformational States for Racemo Dyads, in Syndiotactic and Atactic Stereoisomers at 293 K

Syndiotactic Sequence							
<i>lld</i> – dyad 1–2 ^a			<i>lld</i> – dyad 2–3 ^b				
state ^c	coordinates ^d	F^e	state ^c	coordinates ^d	F^e		
gg	74;69	-0.6(3)	35.3(7)	<i>g[*]g[*]</i>	292;292	0.3(2)	23.7(3)
tg	149;74	2.2(4)	4.2(1)	<i>tg[*]</i>	206;280	2.2(2)	7.32(8)
gt	80;166	1.3(2)	9.7(2)	<i>g[*]t</i>	280;200	2.1(3)	7.1(1)
tt	172;172	0	37.4(4)	<i>tt</i>	189;183	0	51.3(3)
<i>g[*]t</i>	304;154	1.4(3)	6.3(1)	<i>gt</i>	63;200	2.0(2)	3.68(7)
<i>tg[*]</i>	160;304	1.0(3)	7.2(2)	<i>tg</i>	200;52	2.3(2)	7.0(1)

Atactic Sequence							
<i>lld</i> – dyad 2–3 ^b			<i>ddl</i> – dyad 2–3 ^b				
state ^c	coordinates ^d	F^e	state ^c	coordinates ^d	F^e		
gg	69;74	0.7(3)	24.8(4)	<i>g[*]g[*]</i>	292;287	0.2(3)	37.4(4)
tg	154;80	3.0(3)	4.90(8)	<i>tg[*]</i>	212;280	2.4(3)	6.27(8)
gt	92;160	2.7(4)	6.2(1)	<i>g[*]t</i>	287;206	2.4(3)	6.51(8)
tt	166;172	0	55.5(5)	<i>tt</i>	194;183	0	40.5(4)
<i>g[*]t</i>	304;160	2.8(4)	2.72(7)	<i>gt</i>	63;206	2.1(3)	2.78(7)
<i>tg[*]</i>	160;310	2.1(3)	6.0(1)	<i>tg</i>	206;63	1.8(3)	6.5(1)

^aDyad formed by the first and second residues. ^bDyad formed by the second and third residues. ^cRIS nomenclature of the conformational state. States corresponding for symmetry are reported in the same row.

^dAngular coordinates (in degrees) of the absolute minimum of the basin. Pairs $\alpha_1;\alpha_2$ or $\alpha_3;\alpha_4$ for dyads 1–2 or 2–3, respectively. Errors within $\pm 6^\circ$. ^eFree energy (relative to the *tt* state), in kT units. ^fProbability in %.

conformations never correspond to minima, according to the “pentane effect” described by Flory.³⁴ Moreover, we can observe that the minimum free energy dihedral angles in a few cases are shifted from the RIS model values, even of about $\pm 30^\circ$. These shifts, ascribable to the repulsion between the sterically interacting groups, follow a systematic pattern, in a perfect agreement with the behavior prescribed for vinyl polymer chains by Flory et al.³⁵ The differences between conformational features of a dyad, meso or racemo, in stereochemically different chains (see Table 1 or 2) are within the accuracy of the MT simulations.

At 293 K, the meso junction has three accessible conformational states with similar free energies while the racemo junction has six populated minimum free energy states. These findings suggest the syndiotactic sequence owns a more favorable conformational entropy than the isotactic sequence, as reported in a study on the conformational features of the PNIPAAm dimers.³⁹ Even the results of the theoretical treatment of vinyl chain conformation by Flory et al.³⁵ indicate a lower conformational entropy of the isotactic chain in comparison to the syndiotactic one. This characteristic is evinced by the sterical difficulty to intercombine along the chain the two preferred conformational states of the isotactic dyad, corresponding to the two deepest minimum states found in our study, which leads to perpetuate the same dyad conformation in ordered helical sections.³⁵

An important factor for the backbone conformational behavior is given by the extent of free energy barriers between minimum energy states, influencing the kinetics of the dihedral transitions and therefore the system dynamics. At 293 K, the transitions between the three states at the lowest energy of the meso dyad (for example, the states *gt*, *tg**, and *tt* in the maps of Figure 3) have barriers of about 3–6 kT and the transitions between the four states at lower energy of the racemo junction (for example, the states *gg*, *tg*, *tt*, and *gt* in the left map of Figure 1) have barriers of about 3–4 kT. Due to the lower free energy paths between minimum energy conformations, the torsional mobility of the racemo dyad results slightly favored.

The conformational free energy profiles for the stereoisomers of Chart 1 were calculated also at 323 K, a value higher than the LCST of nonstereocontrolled PNIPAMm, that is about 305 K. However, it was recently reported that the stereoregularity of this polymer significantly affects the LCST of its aqueous solution.^{41–44} The LCST of PNIPAAm's with a high meso dyad content (so-called "isotactic-rich PNIPAAm") in water is lower than that of an atactic PNIPAAm.⁴¹ For PNIPAAm's with a meso dyad content of 45 and 66%, LCST's of 304.2 and 290.1 K were found, respectively.⁴² On the contrary, the LCST of a syndiotactic-rich PNIPAAm (with a meso dyad content lower than 45%) in water is higher than that of an atactic PNIPAAm.⁴³ The phase separation temperature is also dependent on the degree of polymerization (DP) of PNIPAAm, and the LCST increases at decreasing DPs and polymer concentrations.^{13,14} Experimental results show that a nonstereocontrolled PNIPAAm trimer, modified with hydrophilic end groups, exhibits a LCST behavior in water for concentrations higher than 30 mg/mL, with a transition temperature of about 323 K.¹⁴ We find that the conformational free energy profiles of all stereoisomers at 323 K present the same minimum energy states observed at 293 K, with a few modifications of the relative population of the conformers, as reported in Part 2 of the Supporting Information. The free energy maps obtained at 323 K, qualitatively similar to those calculated at 293 K, are shown in Part 3 of the Supporting Information.

The occurrence of a temperature influence on the conformational features of $(\text{NIPAAm})_3$ stereoisomers depends on the behavior of the system's enthalpy as a function of the backbone conformation. By considering the *ij* conformational state of a dyad and with ΔF_{ij} being the free energy of the *ij* state relative to the reference state *tt*, the temperature dependence of ΔF_{ij} is described by eq 6

$$\left[\frac{\partial(\Delta F_{ij}/T)}{\partial T} \right]_P = -\frac{\Delta H_{ij}}{T^2} \quad (6)$$

where ΔH_{ij} is the enthalpy difference of the system between the *ij* and *tt* conformational states. Therefore, the influence of the temperature on the relative free energy of a conformational state will be larger, the larger its relative enthalpy. Our results indicate that, both for the meso and racemo dyads, the conformational state basins with lowest free energy do not appreciably change moving from 293 to 323 K (see data in Tables 1 and 2 and in Part 2 of the Supporting Information). Therefore, according to eq 6, these almost isoergonic states own enthalpy and entropy similar to those of the *tt* conformation. On the contrary, when increasing the temperature, a decrease of ΔF_{ij} was found for a few states with a higher free energy, indicating for such states an unfavorable enthalpy contribution (i.e., $\Delta H_{ij} > 0$) due to steric effects. This behavior contributes to make more accessible at increasing temperature all conformational states of the racemo dyad. For the meso dyads, differently, the ΔF_{ij} decrease of some highest free energy (therefore, very scarcely populated) states is not enough to significantly alter the conformer population (see Part 2 of Supporting Information). By and large, these effects globally lead to an increase of the conformational freedom of the racemo dyad at the highest temperature, in comparison to the meso dyad, determining a greater stabilization of the syndiotactic chain in aqueous environment even at 323 K.

A rough estimate of ΔH_{ij} performed using eq 6, provides values around 20 kJ·mol⁻¹ for the *tg* state of racemo dyads and for the *g*t* state of *ll* meso dyads. A positive ΔS_{ij} value is then obtained for such conformations. The higher entropy of these states, with respect to the *tt* conformation, is in agreement with the lower ability to form intramolecular HBs, observed in the MD simulations.

Regarding the free energy barriers, a slight decrease of their heights was found at 323 K, with respect to the values at 293 K. The lack of a marked temperature dependence of the backbone conformation of the dyads in $(\text{NIPAAm})_3$ confirms that the features of the conformational free energy landscapes are mainly determined by the steric hindrances and that the temperature-modulated interaction with the solvent has a lower influence. However, the results of MD simulations showed that the hydrophilicity decrease with temperature acts on the conformation of the less hindered dihedrals of the *N*-isopropyl amide groups, as discussed in section 3.2.

3.2. Molecular Dynamics Simulations. The information obtained from MT-umbrella sampling simulations was implemented by the MD investigation. The MD trajectories were analyzed to investigate both structural and dynamics features of the PNIPAAm trimer in water as a function of chain stereochemistry and temperature.

The conformational behavior of the backbone in the MD simulations agrees with the MT results, and the MT minimum free energy states were observed. In Figure 2a and b, snapshots of the MD trajectories at 293 K show the syndiotactic stereoisomer in two of the most stable conformations, i.e., the *all-trans* and *tt-g*g** conformations. In both of these structures, the *N*-isopropyl amide groups are exposed to water and the *all-trans* conformation can be stabilized by an intramolecular HB between the amide groups of the external residues, as discussed in the following. Two snapshots of the trajectory at 293 K showing *lll* in the most stable conformations *gt-gt* and *tg*-tg** are reported in Figure 2c and d, respectively.

Examples of *ddl* and *lld* structures in minimum free energy conformations from the MD trajectory at 293 K are shown in Figure 5. In Figure 5a, the backbone dihedral states of *ddl* are *tg-tt* and in Figure 5b those of *lld* are *gt-gg*.

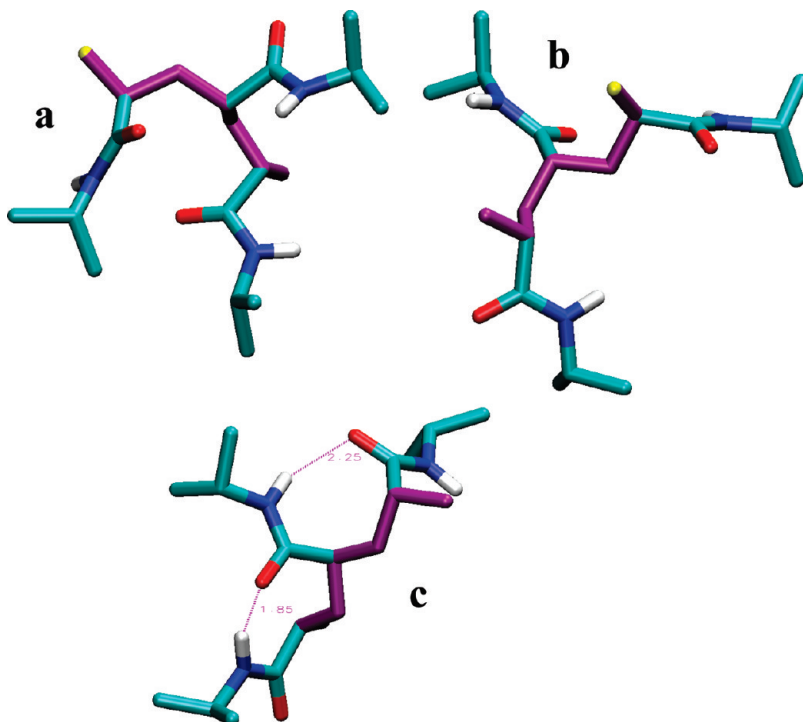


Figure 5. (a) Stereoisomer *ddl* in *tg*–*tt* conformation. (b) Stereoisomer *lld* in *gt*–*gg* conformation. (c) Stereoisomer *lld* in a conformation stabilized by two intradyad HBs. The backbone chain and HBs are shown in purple, with the $\text{H}\cdots\text{O}$ distance in Å. The backbone CP atom is shown in yellow. Snapshots from the MD trajectories at 293 K. The conformation sequence is $\alpha_1\alpha_2-\alpha_3\alpha_4$.

To the aim of highlighting the structural characteristics of the stereoisomers, the hydrogen bond interactions, both intramolecular and with water molecules, eventually stabilizing the preferred conformers, were studied. The presence of intramolecular $\text{C}=\text{O}\cdots\text{H}-\text{N}$ hydrogen bonds in PNIPAAm and in its dimer models even in good solvents was experimentally proved,⁶⁴ and several results suggest that this interaction plays an important role in the phase behavior, as indicated by the different solution behavior between PNIPAAm and poly(*N,N*-diethylacrylamide), a similar but not HB forming polymer.^{65,66} Moreover, a cooperative distribution of HBs between following residues was proposed to stabilize a helical structure of isotactic-rich PNIPAAm in the solvent bis(2-methoxyethyl) ether.⁶⁷ Table 3 reports the characteristics of intramolecular and water–trimer hydrogen bonds for the different stereoisomers under investigation. The hydrogen bonding analysis in the MD trajectories was performed using as geometric criteria for the definition of the $\text{X}-\text{H}\cdots\text{Y}$ hydrogen bond a distance $\text{X}\cdots\text{Y} < 0.35$ nm and an angle $\text{X}\hat{\text{H}}\text{Y} > 120^\circ$, where X and Y are the H donor and acceptor atoms, respectively. The frequency of HBs occurring between specific pairs of residues was calculated, and the results, shown in Table 3, indicate that hydrogen bonds involving amide groups of adjacent residues (i.e., intradyad HBs) are formed both in the meso and in the racemo dyads. The intradyad hydrogen bonding is slightly more frequent for the meso than for the racemo dyads at 293 K, and this difference increases at 323 K, with a HB probability in the meso dyad being about twice than in the racemo dyad. The greater ability of the meso configuration to form intradyad HBs was also reported by Kasumoto et al.,³⁹ in a study of dimer models of PNIPAAm using molecular mechanics calculations.

The HB between amide groups of the first and third residue (i.e., extra-dyad HB) is basically absent in the isotactic

stereoisomer *lll*. On the contrary, extra-dyad HBs are formed in the syndiotactic stereoisomer *lld* and they are particularly relevant in the two atactic trimers *lld* and *ddl*.

It is interesting to relate the results on the intramolecular HBs of our simulations with the findings obtained in an experimental study regarding the rate of hydrogen–deuterium exchange in nonstereocontrolled PNIPAAm of different polymerization degrees in D_2O , at 298 K.³⁸ In the case of the trimer, biphasic kinetics was observed, with two parallel first order processes, the faster one contributing for about one-third of the amide hydrogens and characterized by a rate constant about 5-fold higher than the slower one.³⁸ The authors explained these results by postulating the presence of an intramolecular $\text{C}=\text{O}\cdots\text{H}-\text{N}$ HB between the terminal amide groups, making the H–D exchange process in these groups slower than in the amide of the central residue. In addition, their chromatographic results indicated the presence of only one kind of stereoisomer in the trimer sample used in that study. The data shown in Table 3 agree with this picture, by considering the intramolecular hydrogen bonding of the atactic trimers. In these stereoisomers, the 1–3 HB is present and the ratio between the frequency of HBs involving the first or third residue to that involving the second residue is about 2, a result showing the decreased availability to the H exchange of the external amide groups. This rough evaluation of the kinetic behavior does not take into account the solvent contributions, increasing the difference in reactivity between external and internal amide groups. Such an effect is due to the lower mobility of solvent molecules in the surrounding of the central amide group, observed in MD simulations, which increases the probability of the H exchange reaction.

We investigated the correlation between intramolecular HBs and the backbone conformational state of (NIPAAm)₃

Table 3. Intramolecular and Trimer–Water Hydrogen Bonding^a

stereoisomer	T (K)	intramolecular HBs: percentage of HB existence ^b (%)			trimer–H ₂ O HBs	
		1–2 ^c	2–3 ^c	1–3 ^c	average HB number per residue	HB lifetime ^d (ps)
<i>lld</i>	293	0.66 ± 0.08	0.44 ± 0.05	0.39 ± 0.06	1.83 ± 0.03	7.6 ± 0.6
	323	0.34 ± 0.08	0.33 ± 0.07	0.88 ± 0.02	1.73 ± 0.03	5.0 ± 0.3
<i>lll</i>	293	0.60 ± 0.04	0.47 ± 0.02	0.06 ± 0.03	1.80 ± 0.03	7.6 ± 0.7
	323	0.91 ± 0.05	0.8 ± 0.1	0.009 ± 0.004	1.70 ± 0.03	4.8 ± 0.2
<i>ddl</i>	293	0.7 ± 0.1	0.24 ± 0.01	1.7 ± 0.4	1.80 ± 0.07	7.6 ± 0.7
	323	1.0 ± 0.3	0.33 ± 0.04	1.7 ± 0.1	1.67 ± 0.03	4.9 ± 0.3
<i>lld</i>	293	0.6 ± 0.2	0.35 ± 0.03	1.2 ± 0.3	1.80 ± 0.07	7.6 ± 0.6
	323	0.98 ± 0.01	0.5 ± 0.21	1.7 ± 0.1	1.67 ± 0.03	4.8 ± 0.4

^a Analysis performed on the last 35 ns trajectory of the MD simulations. Averaged values and standard deviations from two independent trajectories.

^b The percentage of existence of the HB between a pair of residues *m*–*n* in the MD trajectory was evaluated as (number of frames with the *m*–*n* HB) · 100/(total number of frames). ^c Pair of residues forming the HB. ^d HB lifetime was evaluated by integration of the corresponding HB autocorrelation function.

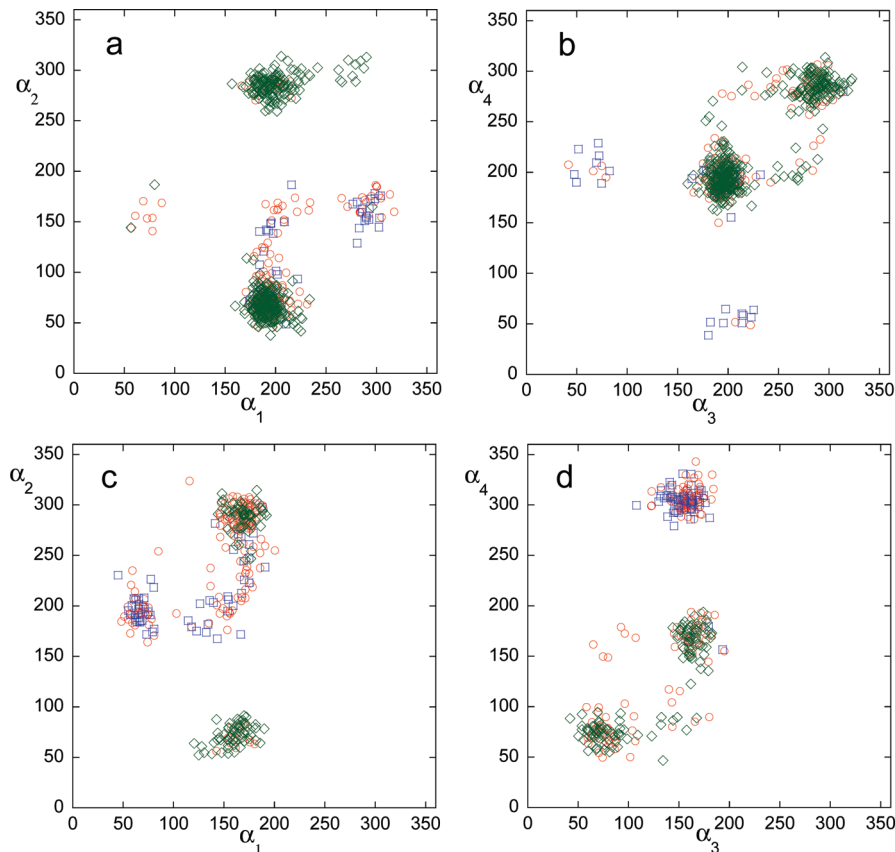


Figure 6. Correlation between backbone conformation and intramolecular HBs at 293 K for *ddl* (a, b) and *lld* (c,d) stereoisomers. The value of the dihedral angle is in degrees. The presence of an intramolecular HB is shown with the symbols: ○ (red, HB between residues 1–2), □ (blue, HB between residues 2–3), ◇ (green, HB between residues 1–3). Trajectory interval: 5–40 ns.

The maps of Figure 6 report the value of the backbone dihedrals in the presence of a HB for the *ddl* and *lld* stereoisomers at 293 K, using different symbols depending on the pair of residues involved in the HB. Figure 6b and d shows that intramolecular HBs are formed in all the minimum free energy states of the racemo dyads (*dl* and *ld*), with a higher HB ability for the *tt* conformation. However, extra-dyad HBs happen only in the domain of the two lowest free energy states (i.e., *tt* and *g*gg*/gg*), contributing to stabilize these conformations. A similar result was

found for the racemo dyads of *lld*. The higher capability of intramolecular hydrogen bonding of the *tt* and *g*gg*/gg* states in the racemo dyad is in agreement with their lower entropy, as estimated from the temperature behavior in the metadynamics simulations. In Figure 6a and c, the intramolecular HBs of the atactic trimers are related with the backbone conformation of the meso dyad. Intradiyad HBs are formed in every meso minimum free energy state, but the extra-dyad HBs are more sterically demanding, needing the α_1 dihedral in trans conformation and

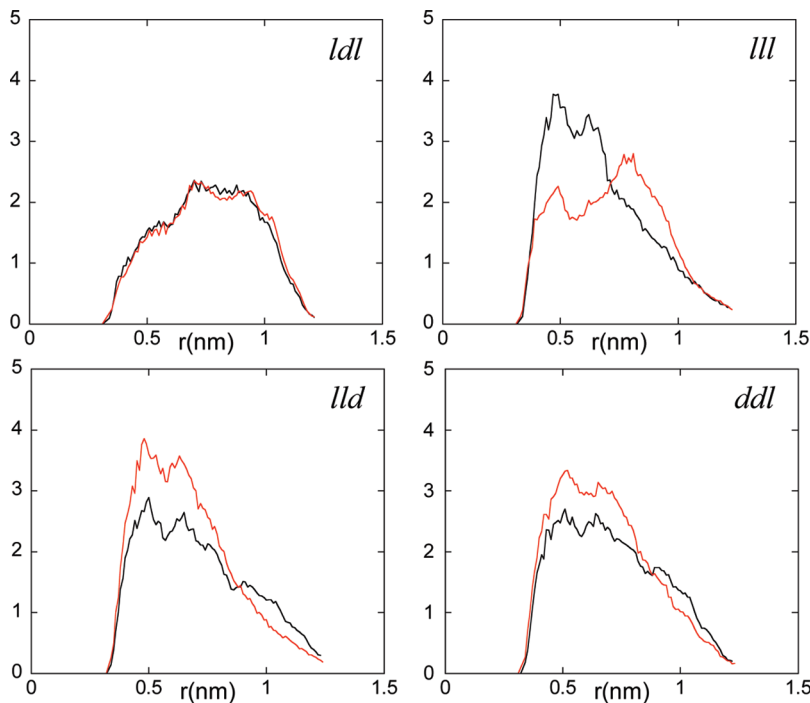


Figure 7. Radial distribution function between carbon atoms of isopropyl groups for the four stereoisomers, at 293 K (black curve) and 323 K (red curve).

the α_2 dihedral in gauche or gauche* conformation. It is noteworthy that the participation of the meso dyad in an extra-dyad HB, practically forbidden in the isotactic chain and favored in the atactic ones, constrains the external backbone dihedral to the trans conformation.

The temperature effect on intramolecular hydrogen bonding is different depending on the chain stereochemistry. In the syndiotactic stereoisomer, *ldl*, the total number of intramolecular HBs does not change with temperature. However, the increase of temperature decreases the intradyad hydrogen bonding and increases the extra-dyad HBs and this behavior leads to stabilize a water exposed, hydrophilic structure even at 323 K, in agreement with the increase of the LCST experimentally observed for syndiotactic-rich PNIPAAm's. For the isotactic stereoisomer, the number of intramolecular HBs at the highest temperature increases, but only intradyad HBs, formed in *gt* and *tg** dyad conformations, are observed. In the *ddl* and *lld* stereoisomers, containing a meso and a racemo dyad, the total number of intramolecular HBs is higher than in the other stereoisomers, at both temperatures, due to the contribution of the extra-dyad HBs. For *ddl* and *lld*, an increase of intramolecular hydrogen bonding with temperature is found even for the racemo dyad.

The formation of an intradyad HB, stabilizing a minimum free energy conformational state of the dyad, is made possible by a suitable relative orientation of the planes containing the amide group. This aspect is governed by the value of the side chain dihedral angle χ_1 , shown in Chart 1, i.e., the torsion angle around the C–C bond between the carbonyl carbon atom of X and the backbone carbon atom CA. In the MD simulations of *III*, *lld*, and *ddl* at the highest temperature, an increase of the side chain conformations leading to intramolecular HBs is observed, without a relevant modification of the backbone conformational behavior.

It is noteworthy that the contribution of intramolecular HBs found in our MD simulations of the trimer is lower than that

experimentally estimated in aqueous solution of PNIPAAm with DP values of about 2000³⁷ and 100.¹⁵ This discrepancy, increasing at increasing PNIPAAm DPs, is ascribable to the higher probability of intramolecular HBs in longer chains.

The trimer–water hydrogen bonding was analyzed by considering the average number of HBs with water *per* (NIPAAm)₃ residue. This value, reported in the sixth column of Table 3, is similar for the different stereoisomers and shows a good accessibility of water to the amide groups at the lowest temperature, taking into account that the maximum number of HBs with water *per* (NIPAAm)₃ residue is three. The increase of temperature slightly depresses the trimer–water hydrogen bonding and accelerates the exchange of the water molecules in the first hydration shell, as shown by the values of the HB autocorrelation time reported in the seventh column of Table 3.

The intra- or interchain hydrogen bonding and the HB with water of PNIPAAm during the coil–globule transition was investigated by FTIR spectroscopy.¹⁵ Above the LCST, about 13% of the C=O groups is estimated to form intra- or interchain HBs and the remaining C=O groups are involved in a HB with water.¹⁵ These results indicate that, on average, above the LCST, one PNIPAAm residue forms about 0.87 HBs with water involving the carbonyl group. Taking into account that a high water content even in the coiled state, corresponding to about 11 water molecules per PNIPAAm residue, was proved by different experimental methods,^{7,16,20} we can admit a HB involvement of the N–H group similar to that of C=O. Therefore, an estimate of about 1.7 HBs *per* residue with water is reliable for PNIPAAm above the LCST. The values of average HB number *per* residue obtained from the MD simulations at 323 K (see Table 3) are in surprising agreement with this experimental evaluation.

A noteworthy temperature effect on the trimer's structure can be observed by considering the arrangement of the hydrophobic

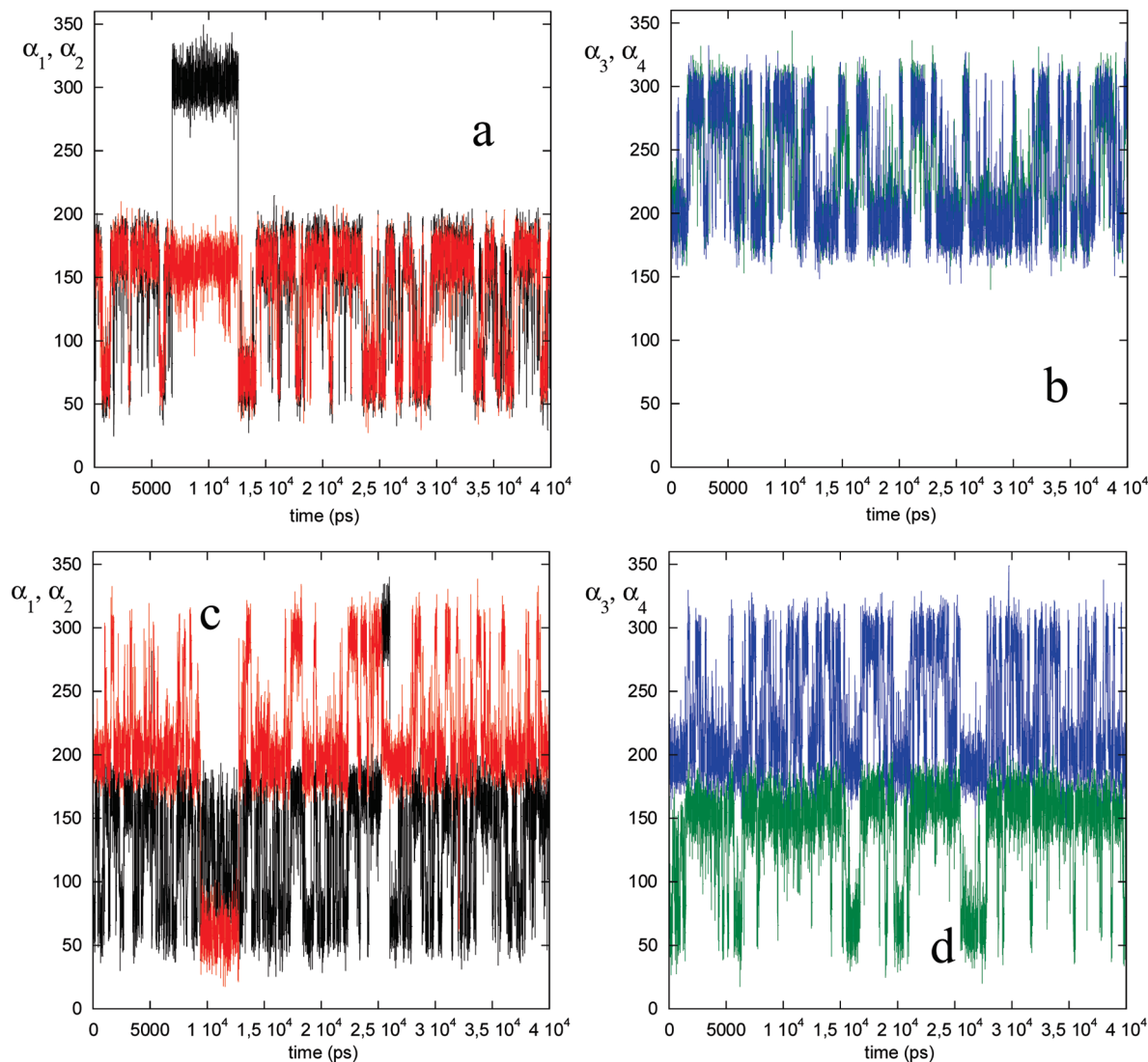


Figure 8. Trajectory of the backbone dihedrals of *ldl* (a and b) and of *lll* (c and d) at 293 K. The dihedrals α_1 , α_2 , α_3 , and α_4 are shown in black, red, green, and blue, respectively. The value of the dihedral angle is in degrees.

Table 4. Torsional Dynamics^a

stereoisomer	$\langle\tau_{\text{rot}}\rangle^b$ (ps) at 293 K				$\langle\tau_{\text{rot}}\rangle^b$ (ps) at 323 K			
	α_1	α_2	α_3	α_4	α_1	α_2	α_3	α_4
<i>ldl</i>	247 ± 27	269 ± 16	200 ± 14	204 ± 28	84 ± 3	109 ± 5	127 ± 5	84 ± 2
<i>lll</i>	104 ± 2	281 ± 19	376 ± 43	134 ± 6	68 ± 1	153 ± 10	241 ± 23	69 ± 6
<i>ddl</i>	126 ± 3	392 ± 11	176 ± 21	168 ± 11	87 ± 6	250 ± 31	127 ± 30	115 ± 9
<i>lld</i>	127 ± 3	399 ± 13	184 ± 9	199 ± 17	81 ± 1	221 ± 30	123 ± 17	119 ± 22

^a Analysis performed on the last 35 ns trajectory. ^b Average lifetime of rotational state, calculated as the trajectory time divided by the number of transitions. Average value and standard deviation over two independent MD simulations.

isopropyl groups. Figure 7 shows the radial distribution function, $g(r)$, between carbon atoms of the isopropyl groups for the four stereoisomers at 293 and 323 K. The sterical relationship between isopropyl groups in the trimer depends on the configuration of the sequence, and for a particular stereoisomer, it is determined by the backbone conformation and by the side chain dihedral angles χ_1 and χ_2 , with the amide dihedral angle ω being

practically fixed in the trans-planar conformation (see Chart 1). From Figure 7, we note that the $g(r)$ of the syndiotactic sequence is unaffected by temperature, whereas in the case of the atactic stereoisomers the $g(r)$ modification at the highest temperature indicates a rearrangement toward an averaged structure with closer hydrophobic groups. These findings are in agreement with the experimental solution behavior of “syndiotactic-rich” and of

nonstereoregular PNIPAAm's. The former, indeed, remains stable in a hydrophilic form in a larger temperature range. The $g(r)$ for the isotactic stereoisomer describes, already at 293 K, an averaged structure with short contacts between hydrophobic groups. The $g(r)$ modification with temperature of *lll* is related to the increased intradyad hydrogen bonding of this stereoisomer at the highest temperature, forcing the system to larger distances between isopropyl groups.

A key element of the local segmental mobility of polymer chains is the torsional dynamics of the backbone, governed by the possibility of transitions between different dihedral conformations. The time evolution of the backbone dihedrals of the syndiotactic stereoisomer is shown in Figure 8a and b. The dihedral dynamics within the dyads of *ldl* is concerted, and the transitions are mainly between the *tt* and *gg* (or g^*g^*) states, the most populated according to the MT results (see Figure 1 and Table 2). From Figure 8a, it can be noted that, in the time interval from about 7 to 12 ns, the *1–2* dyad populates also the g^*t state, where an intradyad HB can be formed.

The time evolution of the backbone dihedrals of the *lll* stereoisomer is shown in Figure 8c and d. The transitions of dihedrals in the meso dyads are less correlated with respect to those in the racemo dyad, and a higher mobility of the external dihedrals, α_1 and α_4 , can be noted. In the transition between the most populated *gt* and *tg** states, the meso dyads populate also a distorted *tt* state, that can be stabilized by an intradyad HB. The torsional dynamics of the meso and racemo dyads in the *ddl* and *lld* isomers is similar to that of the corresponding dyads in the stereoregular isomers.

The average lifetime of conformers for each backbone dihedral is reported in Table 4. The values obtained for the dihedrals of *ldl* are similar, indicating a quite homogeneous torsional mobility of the backbone in the syndiotactic trimer. On the contrary, in *lll*, the external dihedrals are more mobile than the internal ones. In the atactic stereoisomers, the α_2 dihedral has a restricted mobility in comparison to the other backbone dihedrals. This result can be explained taking into account that, only for the atactic trimers, conformations with two simultaneous intramolecular HBs were observed, as shown in Figure 5c. In these structures, the amide group of the central residue, whose orientation depends on the α_2 dihedral, is involved in two HBs as both H donor and acceptor.

The increase of temperature accelerates the torsional dynamics of all stereoisomers. In particular, at 323 K, the syndiotactic stereoisomer displays the highest mobility, a finding in agreement with the lower free energy barriers between conformational states of *ldl*, observed in MT simulations.

CONCLUDING REMARKS

The trimer of PNIPAAm can be considered the shortest oligomer with local dynamical-structural properties close to those of the polymer. The aim of this work is to evaluate, by simulation methods, the effect of stereochemistry on the conformation, structure, and dynamics of $(\text{NIPAAm})_3$ in aqueous solution. The double approach of MT and MD simulations was chosen to obtain complementary information on the system properties. The behavior of the trimer's free energy as a function of backbone conformation showed a higher conformational entropy for the syndiotactic sequence, in comparison to the isotactic one. This characteristic is mainly determined by sterical effects. The amide groups can be involved in intramolecular HBs, contributing to stabilize especially the lowest free energy

conformational states of both the meso and racemo configurations. However, the intramolecular HB connectivity is greater in the stereoisomers with an atactic configuration sequence. In particular, the sterically more demanding HB between amide groups of external residues is more frequent in trimers formed by both a meso and a racemo dyad. In our simulation conditions, corresponding to infinite dilution, the capability to form HB with water molecules is not influenced by stereochemistry. A lower hydrophilicity of the isotactic sequence, in comparison to the syndiotactic one, is shown by the tendency of isopropyl groups of *lll* to cluster at 293 K. The system stereochemistry was found to affect its dynamics. The torsional mobility of the backbone is concerted and homogeneous in the syndiotactic stereoisomer. On the contrary, in the isotactic stereoisomer, the chain-ends are more mobile than the central domain. These results suggest that even in longer chains the isotactic sequence owns a decreased mobility with respect to the syndiotactic one. Such a property could facilitate the intramolecular aggregation and the precipitation of the polymer from the aqueous solution at lower temperature.

The increase of temperature does not influence the lowest free energy conformational states of the backbone, in the temperature range investigated. A temperature effect is observed on the side chain conformations, leading to an increase of intramolecular HBs of all, but the syndiotactic, stereoisomers. Our MD simulation conditions "a priori" do not allow one to observe the hydrophobic aggregation process, which causes the phase separation at increasing temperature. However, the evolution toward a less hydrophilic structure at increasing temperature was observed in the case of the atactic stereoisomers. These findings indicate that the transition from relaxed coil to globule of PNIPAAm above the LCST involves small modifications of backbone dihedrals in residues separated by more than two repeating units.

Several factors contribute to define the phase behavior of PNIPAAm in water: concentration, polymer length, polydispersity, and stereochemistry. Between them, the concentration and DP effects become progressively less relevant at increasing polymer length.^{12–14,16} According to the opinion of Katsumoto et al.,⁴⁴ who compared the phase behavior of atactic and isotactic-rich PNIPAAm's having similar DP and polydispersity and the phase behavior of atactic PNIPAAm's with DP of about 300 and 6000, the effect of the tacticity on the phase boundary curve is much larger than that of the molecular weight. This conclusion was one of the motivations of our study.

The results of this simulation work are in agreement with available experimental data on solution and reactivity properties of PNIPAAm in water. These findings, providing an atomic detailed description of structure and dynamics, can contribute to highlight the peculiar characteristics of PNIPAAm in relation to its stereochemistry. The interpretation of experimental data regarding the local structure and dynamics of stereocontrolled PNIPAAm's could be supported by information here reported, in particular in the case of experiments based on quasi-elastic neutron scattering,⁶⁸ a technique sampling the same time-space domain of MD simulations.

ASSOCIATED CONTENT

S Supporting Information. Part 1, a figure showing the free energy maps of the *ddl* stereoisomer at 293 K; part 2, two tables with the minimum free energy conformational states, their relative free energy and population at 323 K for meso and racemo dyads of systems studied; part 3, four figures showing the free

energy maps obtained at 323 K. This material is available free of charge via the Internet at <http://pubs.acs.org>.

AUTHOR INFORMATION

Corresponding Author

*E-mail: ester.chiessi@uniroma2.it.

ACKNOWLEDGMENT

This work was partially funded by MIUR project PRIN 20077LCNTW. The authors thank CNISM/CINECA for supplying high performance computing facilities and acknowledge the use of computing time at the Wiglaf HPC cluster of the Department of Physics of the University of Trento.

REFERENCES

- (1) Sprecht, E. H.; Neuman, A.; Neher, H. T. U.S. Patent 2,773,063, 1956.
- (2) CIBA Ltd. Br. Patent 746,747, 1956.
- (3) Sprecht, E. H.; Neuman, A.; Neher, H. T. Br. Patent 772,196, 1956.
- (4) Shearer, N. H., Jr.; Coover, H. W., Jr. U.S. Patent 2,790,744-5, 1957.
- (5) Schild, H. G. *Prog. Polym. Sci.* **1992**, *17*, 163.
- (6) Graziano, G. *Int. J. Biol. Macromol.* **2000**, *27*, 89.
- (7) (a) Wang, X.; Qiu, X.; Wu, C. *Macromolecules* **1998**, *31*, 2972.
(b) Wu, C.; Wang, X. *Phys. Rev. Lett.* **1998**, *80*, 4092.
- (8) Naddaf, A. A.; Tsibranska, I.; Bart, H.-J. *Chem. Eng. Process.* **2010**, *49*, 581.
- (9) Wei, H.; Cheng, S.-X.; Zhang, X.-Z.; Zhuo, R.-X. *Prog. Polym. Sci.* **2009**, *34*, 893.
- (10) Aoshima, S.; Kanaoka, S. *Adv. Polym. Sci.* **2008**, *210*, 169.
- (11) Fairve, M.; Campillo, C.; Pepin-Donat, B.; Viallat, A. *Prog. Colloid Polym. Sci.* **2006**, *133*, 41.
- (12) Afroze, F.; Nies, E.; Berghmans, H. *J. Mol. Struct.* **2000**, *554*, 55.
- (13) Pamies, R.; Zhu, K. Z.; Kjøniksen, A. L.; Nyström, B. *Polym. Bull.* **2009**, *62*, 487.
- (14) Shan, J.; Zhao, Y.; Granqvist, N.; Tenhu, H. *Macromolecules* **2009**, *42*, 2696.
- (15) Maeda, Y.; Higuchi, T.; Ikeda, I. *Langmuir* **2000**, *16*, 7503.
- (16) Ono, Y.; Shikata, T. *J. Am. Chem. Soc.* **2006**, *128*, 10030.
- (17) Hidaka, M.; Yoshida, R. *J. Controlled Release* **2011**, *150*, 171.
- (18) Ekici, S. *J. Mater. Sci.* **2011**, *46*, 2843.
- (19) Malmsten, M.; Bysell, H.; Hansson, P. *Curr. Opin. Colloid Interface Sci.* **2010**, *15*, 435.
- (20) Geukens, B.; Meersman, F.; Nies, E. *J. Phys. Chem. B* **2008**, *112*, 4474.
- (21) Lai, H.; Wu, P. *Polymer* **2010**, *51*, 1404.
- (22) Longhi, G.; Lebon, F.; Abbate, S.; Fornili, S. L. *Chem. Phys. Lett.* **2004**, *386*, 123.
- (23) Gangemi, F.; Longhi, G.; Abbate, S.; Lebon, F.; Cordone, R.; Ghilardi, G. P.; Fornili, S. L. *J. Phys. Chem. B* **2008**, *112*, 11896.
- (24) Chiessi, E.; Lonardi, A.; Paradossi, G. *J. Phys. Chem. B* **2010**, *114*, 8301.
- (25) Tamai, Y.; Tanaka, H.; Nakanishi, K. *Macromolecules* **1996**, *29*, 6750.
- (26) Tamai, Y.; Tanaka, H.; Nakanishi, K. *Macromolecules* **1996**, *29*, 6761.
- (27) Tönsing, T.; Oldiges, C. *Phys. Chem. Chem. Phys.* **2001**, *3*, 5542.
- (28) Walter, J.; Ermatchkov, V.; Vrabec, J.; Hasse, H. *Fluid Phase Equilib.* **2010**, *296*, 164.
- (29) Pang, J.; Yang, H.; Ma, J.; Cheng, R. *J. Phys. Chem. B* **2010**, *114*, 8652.
- (30) Zhang, G.; Wu, C. *J. Am. Chem. Soc.* **2001**, *123*, 1376.
- (31) Ramachandran, G. N.; Ramakrishnan, C.; Sasisekharan, V. *J. Mol. Biol.* **1963**, *7*, 95.
- (32) Brant, D. A. *Q. Rev. Biophys.* **1976**, *9*, 527.
- (33) Olson, W. K.; Flory, P. J. *Biopolymers* **1972**, *11*, 25–56.
- (34) Abe, A.; Jernigan, R. L.; Flory, P. J. *J. Am. Chem. Soc.* **1966**, *88*, 631.
- (35) Flory, P. J.; Mark, J. E.; Abe, A. *J. Am. Chem. Soc.* **1966**, *88*, 639.
- (36) Flory, P. J. *Macromolecules* **1974**, *7*, 381.
- (37) Scarpa, J. S.; Mueller, D. D.; Klotz, I. M. *J. Am. Chem. Soc.* **1967**, *89*, 6024.
- (38) Snyder, W. D.; Klotz, I. M. *J. Am. Chem. Soc.* **1975**, *97*, 4999.
- (39) Katsumoto, Y.; Kubasaki, N.; Miyata, T. *J. Phys. Chem. B* **2010**, *114*, 13312.
- (40) Isobe, Y.; Fujioka, D.; Habaue, S.; Okamoto, Y. *J. Am. Chem. Soc.* **2001**, *123*, 7180.
- (41) Suito, Y.; Isobe, Y.; Habaue, S.; Okamoto, Y. *J. Polym. Sci., Part A: Polym. Chem.* **2002**, *40*, 2496.
- (42) Ray, B.; Okamoto, Y.; Kamigaito, M.; Sawamoto, M.; Seno, K.; Kanaoka, S.; Aoshima, S. *Polym. J.* **2005**, *37*, 234.
- (43) Hirano, T.; Okumura, Y.; Kitajima, H.; Seno, M.; Sato, T. *J. Polym. Sci., Part A: Polym. Chem.* **2006**, *44*, 4450.
- (44) Katsumoto, Y.; Kubasaki, N. *Macromolecules* **2008**, *41*, 5955.
- (45) Brooks, B. R.; Brooks, C. L., 3rd; Mackerell, A. D., Jr; Nilsson, L.; Petrella, R. J.; Roux, B.; Won, Y.; Archontis, G.; Bartels, C.; Boresch, S.; Caflisch, A.; Caves, L.; Cui, Q.; Dinner, A. R.; Feig, M.; Fischer, S.; Gao, J.; Hodoscek, M.; Im, W.; Kuczera, K.; Lazaridis, T.; Ma, J.; Ovchinnikov, V.; Paci, E.; Pastor, R. W.; Post, C. B.; Pu, J. Z.; Schaefer, M.; Tidor, B.; Venable, R. M.; Woodcock, H. L.; Wu, X.; Yang, W.; York, D. M.; Karplus, M. *J. Comput. Chem.* **2009**, *30*, 1545.
- (46) Berendsen, H. J. C.; Postma, J. P. M.; van Gunsteren, W. F.; Hermans, J. *Intermolecular Forces*; Reidel: Dordrecht, The Netherlands, 1981; pp 331–342.
- (47) Schuler, L. D.; van Gunsteren, W. F. *Mol. Simul.* **2000**, *25*, 301.
- (48) Schuler, L. D.; Daura, X.; van Gunsteren, W. F. *J. Comput. Chem.* **2001**, *22*, 1205.
- (49) Lindahl, E.; Hess, B.; van der Spoel, D. *J. Mol. Model.* **2001**, *7*, 306.
- (50) van der Spoel, D.; Lindahl, E.; Hess, B.; Groenhof, G.; Mark, A. E.; Berendsen, H. J. C. *J. Comput. Chem.* **2005**, *26*, 1701.
- (51) Hockney, R. W. *Methods Comput. Phys.* **1970**, *9*, 136.
- (52) Hess, B.; Bekker, H.; Berendsen, H. J. C.; Fraaije, J. G. E. M. *J. Comput. Chem.* **1997**, *18*, 1463.
- (53) Berendsen, H. J. C.; Postma, J. P. M.; van Gunsteren, W. F.; Di Nola, A.; Haak, J. R. *J. Chem. Phys.* **1984**, *81*, 3684.
- (54) Essmann, U.; Perera, L.; Berkowitz, M. L.; Darden, T.; Lee, H.; Pedersen, L. G. *J. Chem. Phys.* **1995**, *103*, 8577.
- (55) Humphrey, W.; Dalke, A.; Schulter, K. *J. Mol. Graphics* **1996**, *14*, 33.
- (56) Bussi, G.; Laio, A.; Parrinello, M. *Phys. Rev. Lett.* **2006**, *96*, 090601.
- (57) Laio, A.; Gervasio, F. L. *Rep. Prog. Phys.* **2008**, *71*, 126601.
- (58) Barducci, A.; Bussi, G.; Parrinello, M. *Phys. Rev. Lett.* **2008**, *100*, 020603.
- (59) Babin, V.; Roland, C.; Darden, T. A.; Sagui, C. *J. Chem. Phys.* **2006**, *125*, 204909.
- (60) Autieri, E.; Segà, M.; Pederiva, F.; Guella, G. *J. Chem. Phys.* **2010**, *133*, 095104.
- (61) Bonomi, M.; Branduardi, D.; Bussi, G.; Camilloni, C.; Provasi, D.; Raiteri, P.; Donadio, D.; Marinelli, F.; Pietrucci, F.; Broglia, R. A.; Parrinello, M. *Comput. Phys. Commun.* **2009**, *180*, 1961.
- (62) Hess, B.; Kutzner, C.; van der Spoel, D.; Lindahl, E. *J. Chem. Theory Comput.* **2008**, *4*, 435.
- (63) Berendsen, H. J. C.; van der Spoel, D.; Van Drunen, R. *Comput. Phys. Commun.* **1995**, *91*, 43.
- (64) Katsumoto, Y.; Tanaka, T.; Ihara, K.; Koyama, M.; Ozaki, Y. *J. Phys. Chem. B* **2007**, *111*, 12730.
- (65) Maeda, Y.; Nakamura, T.; Ikeda, I. *Macromolecules* **2002**, *35*, 10172.
- (66) Kobayashi, M.; Ishizone, T.; Nakahama, S. *J. Polym. Sci., Part A: Polym. Chem.* **2000**, *38*, 4677.
- (67) Koyama, M.; Hirano, T.; Ohno, K.; Katsumoto, Y. *J. Phys. Chem. B* **2008**, *112*, 10854.
- (68) Chiessi, E.; Cavalieri, F.; Paradossi, G. *J. Phys. Chem. B* **2007**, *111*, 2820.